Photoionization cross section and intersublevel transitions in a one- and two-electron spherical quantum dot with a hydrogenic impurity

Mehmet Şahin*
Selçuk University, Faculty of Sciences and Arts, Physics Department, Kampüs 42075 Konya, Turkey
(Received 19 September 2006; revised manuscript received 7 February 2007; published 17 January 2008)

A detailed investigation of the optical properties of a spherical quantum dot (QD) containing one and two electrons has been performed for cases with and without a hydrogenic impurity. First, the photoionization cross section of both D^0 and D^- impurities in the QD has been calculated for an on-center impurity. Second, the intersublevel optical absorption and oscillator strength between the ground and excited states have been examined based on the computed energies and wave functions. The full numeric matrix diagonalization technique has been employed in determining sublevel energy eigenvalues and their wave functions. The Poisson-Schrödinger equations have been solved self-consistently in the Hartree approximation. In addition, quantum-mechanical many-body effects have been investigated in the local density approximation. The results are presented as a function of quantum dot radii and photon energies.

DOI: 10.1103/PhysRevB.77.045317 PACS number(s): 73.20.Mf, 73.21.La, 78.67.Hc

I. INTRODUCTION

Recent improvements in the fabrication of low-dimensional systems have made it possible to prepare nanoscale semiconductor heterostructures in which the carriers are confined in their motion in one, two, and three dimensions such as quantum wells, quantum wires, and quantum dots.[1,2] Detailed descriptions of these structures have been presented in Ref. 2. These semiconductor quantum nanostructures have found various application areas especially as electronic and optoelectronic devices such as single-electron transistors and quantum well and quantum dot infrared photodetectors (QWIP and QDIP).[3–5] Therefore, these structures have been intensively studied both theoretically and experimentally in condensed matter and applied physics.[6–9]

Serious attention has recently been focused on the zero-dimensional quantum dot (QD), also called an artificial atom because it exhibits atomic properties, for optoelectronic devices due to their advantages over quantum wells. Hence, optical properties of QDs have been investigated both experimentally and theoretically by many authors.[9–14]

The electronic states are very sensitive to the size of QDs. The number of electrons in the QD is also very important for many physical properties of these structures, since with increasing number of electrons the electron-electron interaction becomes important and it changes the effective potential. As the electron-electron interaction pushes up the energy levels, a donor impurity pulls down these levels a little. Consequently, the confining potential, number of electrons, and existence of impurities in the QDs affect drastically the electronical and optical properties of these structures. A number of studies have been reported on many-electron effects in semiconductor QDs.[6,12]

The hydrogenic impurity problem in a low-dimensional systems is a very useful model for understanding the electronic and optical properties of these heterostructures—for example, donor binding energy, electronic structure in electric and magnetic fields, photoionization cross section, and other optical properties. Hence, they have been studied by many authors.[6,11,15–20]

The photoionization cross section of a hydrogenic impurity in low-dimensional structures is also studied widely by many authors.[21–36] The cross section depends strongly on the impurity binding energy and its wave function.[21] The photoionization cross section of a hydrogenic impurity in bulk semiconductors was first investigated by Lax.[22] Takikawa *et al.*[23] examined the photoionization cross section associated with a transition from a deep trap to subbands theoretically and experimentally. Ilaiwi and Tomak[24] investigated the dependence of the photoionization cross section on photon energy for bulk impurities using different impurity potentials. El-Said and Tomak[25] calculated the photoionization cross section for shallow donors in an infinite-barrier quantum well as a function of excitation energy, well width, and applied magnetic field. They researched also light polarization effect in another study.[26] El-Kawni and Tomak[27] extended these calculations to heterojunctions using the both infinite and finite confining potentials under different physical conditions. Ilaiwi and El-Said[28] studied the dependence of the photoionization cross section on photon energy for shallow donors as a function of well width and magnetic field in finite-barrier quantum wells. Sali *et al.*[29] investigated the photon energy dependence of the photoionization cross section for a hydrogenic impurity in a quantum wire for several values of the confining potential. Later, Sali *et al.*[30] examined the photon energy dependence of the photoionization cross section in an infinite-barrier quantum box as a function of size and impurity position using a variational approach. Ham and Spector[21] analyzed the dependence of the photoionization cross section on the energy and polarization of the photons in a spherical QD as a function of dot radius and impurity locations for both infinite and finite potential barriers. They found that the cross section is independent of the polarization of the photons for an on-center impurity while it depends on the polarization of the photon field for an off-center impurity. Ham and Lee[31] researched the cross section of a hydrogenic impurity in a cylindrical quantum wire using an infinite-well model. Recently, Kasapoglu *et al.*[32,33] carried out an investigation of the effect of the electric, magnetic, and intense laser fields and also hydrostatic pressure on the

photoionization in quantum well wires. The photoionization cross section is still studied extensively under different physical conditions in low-dimensional systems.[34–36]

Bound-to-bound transitions between intersublevels in a QD are very important for device applications such as QDIPs, and many theoretical works reported on photon absorption properties between intersublevels in QDs.[4,11–14,37–39] Although a detailed investigation of the intersublevel optical spectrum of a neutral donor (D^0) has been performed by Buczko and Bassani,[11] the absorption spectra of a negatively charged (D^-) impurity in a QD has still not been investigated.

All of these studies are related to a D^0. In the neutral hydrogenic donor the problem contains only one electron and, therefore, the solution of this problem is not complex and it can be easily solved by traditional variational methods. Nevertheless, a D^- structure has two electrons and the Coulomb interaction between the electrons must be taken into consideration in the calculations. Therefore, the solving of a D^- problem is not so simple as a D^0 problem. Up to now, neither the photoionization cross section of a D^- impurity nor intersublevel transitions of that has been investigated.

The main goal of this study is to investigate the detailed optical properties of one- and two-electron spherical quantum dots with and without a hydrogenic impurity. In this work, the photoionization cross section of a D^0 and a D^- center is examined as a function of the dot radius and the normalized photon energy. On the other hand, investigations of the optical transitions and the oscillator strengths are carried out between the intersublevels in a spherical QD depending on the number of electrons for cases with and without the impurity. The Poisson-Schrödinger equations are solved self-consistently in the Hartree approximation for determining the energies and the wave functions of the D^- center. The many-body quantum mechanical effect is also taken into account in the local density approximation (LDA).

This paper is organized as follows: In the next section, details of the calculations are presented. Results and discussions are given in Sec. III as separated for photoionization and absorption. In the last section, a brief conclusion is given.

II. DETAILS OF THE CALCULATIONS

In the calculations, Hartree and local density approximations are used to determine the electronic states of double-electron cases. Actually, the Kohn-Sham equations have the same form as the Hartree equations. Both of them are basically an $\hat{H}\phi=E\phi$ eigenvalue equation and depend on the Poisson-Schrödinger equations being solved self-consistently. The main difference between them is to be considered the quantum-mechanical many-body effect in the Kohn-Sham density functional theory, and so more computational effort for Kohn-Sham calculations is not required.[40]

The Hartree approximation supposes that one electron moves in a mean potential field created by other electron(s) in a many-electron system.[41–43] Although this model is quite simple, its results are accurate enough in the understanding of more properties of a many-electron system and it is used widely.

Quantum-mechanical exchange-correlation (XC) effects can be taken into consideration for more accurate calculations beyond the Hartree approximation. Different kinds of approximations are employed for the XC potential—for instance, LDA, generalized gradient approximation (GGA), local spin density approximation (LSDA), etc. As is well known, these types of approximations work better when the particle number goes to thermodynamics limits. However, when the electron numbers are $N=2,3,4,\ldots,10$, these approximations are widely and successfully used in the calculations.[6,12,44,45]

An atomistic calculation is a valuable tool for the calculation, investigation, and understanding of the microscopic properties of materials in condensed matter physics. There are several methods available—Monte Carlo, molecular dynamics, lattice dynamics, energy-force minimization, etc. Nevertheless, all of these methods depend on a knowledge of the interatomic potential and it is not very easy to know this potential.[46]

A. Model and theory

In this study, a spherically symmetric quantum dot with radius R_{dot}, which is embedded in a bulk semiconductor, is considered. The effective mass approximation and BenDaniel-Duke boundary conditions are used for the self-consistent calculations. In the effective mass approximation, for a spherically symmetric N-electron quantum dot with radius R_{dot} the single-particle Schrödinger equation is given as

$$\left[-\frac{\hbar^2}{2}\vec{\nabla}_r\left(\frac{1}{m^*(r)}\vec{\nabla}_r\right)-\frac{Ze^2}{|\vec{r}-\vec{r}_i|}+\frac{\ell(\ell+1)\hbar}{2m^*(r)r^2}-e\Phi_{e\text{-}e}+V_b+V_{xc}\right]R_{n,\ell}(r)=\varepsilon_i R_{n,\ell}(r). \quad (1)$$

Here, $\hbar^2$ is the reduced Planck constant, $m^*(r)$ is the position-dependent electron's effective mass, Z is the charge of the impurity, ℓ is the angular momentum quantum number, $\Phi_{e\text{-}e}$ is the electrostatic potential between the electrons, V_b is the finite confining potential, $\varepsilon_{n,\ell}$ is the single-particle energy eigenvalue, $R_{n,\ell}(r)$ is the radial wave functions of these particles, and V_{xc} is the exchange-correlation potential. The exchange-correlation potential and the Coulomb potential between electrons are not considered in one-electron cases since there are no other electron(s) for these kinds of interactions. In cases of more than one electron, the electron-electron Coulomb interaction potential is determined from the Poisson equation

$$\nabla^2\Phi_{e\text{-}e}=\frac{e\rho_e(r)}{\kappa(r)}, \quad (2)$$

where $\rho_e(r)$ is the electron density and $\kappa(r)$ is the dielectric constant of the structure. The electron density is

$$\rho_e(r) = \frac{1}{4\pi}\sum_{\ell=0}^{p} 2(2\ell+1)\sum_{n=1}^{np} |R_{n,\ell}(r)|^2, \quad (3)$$

where $2(2\ell+1)$ is the spin and magnetic degeneracies, and p and np are the angular momentum quantum number and the principle quantum number of the occupied states, respectively. Here, the maximum electron number is $N=2$, and so only the $1s$ shell is fully occupied with the electrons.

For the exchange-correlation potential, the Perdew-Zunger[47] expression, which is a parametrization of the Monte Carlo results of Ceperley and Alder,[48] is employed. Also, this formulation contains a self-interaction correction.

In order to determine the single-particle energy levels and corresponding wave functions, Eqs. (1)–(3) are solved self-consistently in the Hartree or local density approximation. It should be noted that when just the Hartree approximation is employed in the calculations, the exchange-correlation potential V_{xc} is taken as zero in Eq. (1). The matrix diagonalization technique is used for the determination of the single-particle energies and corresponding eigenfunctions. For this purpose, the Hamiltonian operator is discretized on a uniform radial mesh in one dimension (1D) using the finite difference technique; then, Eq. (1) can be reduced to a matrix eigenvalue equation. Here, the width Δr between two mesh points is chosen as 0.008. Eigenvalues and eigenvectors of this matrix equation are determined by the EISPACK subroutine. These eigenvectors are used in Eq. (3) for determining the charge density. The charge density in turn is used in the exchange-correlation potential and Poisson equation (2), and thus the electrostatic potential $\Phi_{e\text{-}e}$ is calculated. The finite-difference technique with Gauss elimination method is used for the calculation of this potential. In order to perform a self-consistent calculation, this electrostatic potential and exchange-correlation potential are substituted into Eq. (1) and this process is continued until it converges.

B. Theory of the photoionization cross section

The photoionization process is an optical transition that takes place from the impurity ground state as the initial state to the conduction subbands (continuum), which starts above the confining potential of the dot. It requires sufficient energy in order for the transition to occur.[30] The photoionization cross section can be defined as the ionization probability of the electrons from the bound state under an external optical excitation. It is strongly dependent on the confinement potential and the photon energy. The excitation energy dependence of the photoionization cross section associated with an impurity, starting from Fermi's golden rule in the well-known dipole approximation, as in the bulk case, is[22,30]

$$\sigma(\hbar\omega) = \left[\left(\frac{F_{eff}}{F_0}\right)^2 \frac{n_r}{\kappa}\right]\frac{4\pi^2}{3}\beta_{FS}\hbar\omega\sum_f |\langle\psi_i|\mathbf{r}|\psi_f\rangle|^2 \times \delta(E_f - E_i - \hbar\omega), \quad (4)$$

where n_r is the refractive index of the semiconductor, κ is the dielectric constant of the medium, $\beta_{FS}=e^2/\hbar c$ is the fine structure constant, and $\hbar\omega$ is the photon energy. F_{eff}/F_0 is the ratio of the effective electric field F_{eff} of the incoming photon and average field F_0 in the medium.[49] $\langle\psi_i|\mathbf{r}|\psi_f\rangle$ is the matrix element between the initial and final states of the dipole moment of the impurity. ψ_f and ψ_i are the wave function of the final and initial states, and E_f and E_i are the corresponding energy eigenvalues to these states, respectively. These eigenvalues and eigenvectors are determined by self-consistent solution of the Poisson-Schrödinger equations.

In spherical QDs, the selection rules ($\Delta\ell = \pm 1$) determine the final state of the electron after the impurity photoionization. The $1s$ impurity state is taken as the ground level for both D^0 and D^- and the $1p$ level of a one- (two-) electron system without the impurity is considered as the final state for D^0 (D^-) as similar with other studies[21,34,50] and details of the physical reasons of this approximation have been explained in those studies.[25–30]

In order to calculate the numerical values of the photoionization cross section given by Eq. (4), F_{eff}/F_0 is taken as approximately unity because the calculation of this quantity is very difficult and it has no effect on the photoionization cross-section shape.[24–27,30] Also, the initial- and final-state wave functions (ψ_i and ψ_f) are determined by the multiplication of the radial wave function with the spherical harmonics—i.e., $R_{n,\ell}(r)Y_{\ell,m}(\theta,\varphi)$. Here, $Y_{\ell,m}(\theta,\varphi)$ is the spherical harmonics. In addition, the δ function in Eq. (4) is replaced by a narrow Lorentzian by means of

$$\delta(E_f - E_i - \hbar\omega) = \frac{\hbar\Gamma}{\pi\{[\hbar\omega - (E_f - E_i)]^2 + (\hbar\Gamma)^2\}}. \quad (5)$$

Here, Γ is the hydrogenic impurity linewidth and taken as $0.1R_y^*$.

C. Theory of intersublevel transitions

In low-dimensional quantum-mechanical systems, the photoabsorption process can be described as an optical transition that occurs from a lower state to an upper state with absorbing a photon. The optical absorption calculations for the intersublevel are based on Fermi's golden rule which is a result of time-dependent perturbation theory and the intersublevel optical absorption coefficient is given by[51]

$$\alpha(\hbar\omega) = \frac{8\pi e^2\beta_{FS}N_{if}}{n_r V_{QD}}\hbar\omega|z_{if}|^2\delta(E_f - E_i - \hbar\omega), \quad (6)$$

where n_r is the refractive index of the semiconductor and it is taken as 3.15, V_{QD} is the QD volume, $\beta_{FS}=e^2/\hbar c$ is the fine structure constant, and $\hbar\omega$ is the photon energy. $N_{if}=N_i-N_f$ where N_i and N_f are the number of the electrons in the initial and final states, respectively. Also, E_f and E_i are the final- and initial-state energy eigenvalues, respectively.

The selection rules determine the final state of the electron after the absorption. Hence, the $1s$ state is taken as the ground level and the $1p$ level is taken as the final state.

The polarization of the electromagnetic radiation is chosen as the z direction. The z_{if} in Eq. (6) is the transition matrix element between the initial and final states, and it is defined as

$$|z_{if}|^2 = |\langle \psi_f | z | \psi_i \rangle|^2. \tag{7}$$

This equation can be written in terms of radial and spherical parts of the wave function as

$$|z_{if}|^2 = \left| \int R_{n'\ell'}(r) r R_{n\ell}(r) r^2 dr Y_{\ell' m'}(\theta,\varphi) \cos(\theta) Y_{\ell m}(\theta,\varphi) \sin(\theta) d\theta d\varphi \right|^2, \tag{8}$$

and for $\ell'=1$, $\ell=0$ and $m'=m=0$, the matrix element becomes

$$|z_{if}|^2 = \frac{1}{3} \left| \int_0^\infty R_{1,1}(r) r^3 R_{1,0}(r) dr \right|^2. \tag{9}$$

The δ function in Eq. (6) is replaced by a narrow Lorentzian by means of Eq. (5) and the Lorentzian linewidth Γ is taken as 10 meV.

A physical quantity of practical importance in the study on the optical properties is the dimensionless oscillator strength P_{fi}, which is defined by

$$P_{fi} = \frac{2m^*}{\hbar^2} (E_f - E_i) |z_{if}|^2, \tag{10}$$

$$P_{fi} = \frac{2m^*}{3\hbar^2} (E_f - E_i) \left| \int_0^\infty R_{1,1}(r) r^3 R_{1,0}(r) dr \right|^2. \tag{11}$$

III. NUMERICAL RESULTS AND DISCUSSION

In most of the theoretical studies on spherical quantum dots, the authors use the material parameters of GaAs for the well region and that of AlGaAs for the barrier region,[6,7,11,12,14,16,17,21] because their basic physical properties such as band mismatch, effective masses, and dielectric constants are better known.[52] Hence, these material parameters are used and detailed results are given for the GaAs/AlGaAs quantum dot.

Atomic units have been used throughout the calculations, where the Planck constant $\hbar=1$, the electronic charge $e=1$, and the electron mass $m=1$. The effective Bohr radius is $a_0^*=100$ Å and the effective Rydberg energy is $R_y^*=5.75$ meV. The material parameters have been taken as $m_{\mathrm{GaAs}}=0.067m_0$, $m_{\mathrm{AlGaAs}}=0.088m_0$, $V_b=228$ meV, $\kappa_{\mathrm{GaAs}}=13.11$, and $\kappa_{\mathrm{AlGaAs}}=12.8$. Also the effective masses of electrons inside GaAs and AlGaAs are m_1^* and m_2^*, and the dielectric constants are κ_1 and κ_2, respectively. The position-dependent effective mass and the dielectric constant may be defined as follows:[11]

$$m^*(r) = \begin{cases} 1, & r < R_{dot}, \\ \dfrac{m_2^*}{m_1^*}, & r > R_{dot}, \end{cases} \qquad \kappa(r) = \begin{cases} 1, & r < R_{dot}, \\ \dfrac{\kappa_2}{\kappa_1}, & r > R_{dot}. \end{cases} \tag{12}$$

The Coulomb potential due to the impurity has a singularity at $r=0$. In order to avoid the numerical singularity of the impurity potential at the origin of the QD, the cusp condition,[53] which modifies the eigenfunctions so as to take into account the effect of the singularity, is used.

As is well known, if the radius of the dot with a hydrogenic impurity is large enough, one electron in the dot is bound to this hydrogenic impurity and the structure is known as a neutral donor impurity (D^0).[16,17] Moreover, if the radius becomes larger, a second electron also can bind as a result of polarization. In this case, the structure is called a negatively charged (D^-) impurity.[54,55] The binding energy of a neutral donor impurity is the difference between the total energies for cases with ($Z=1$) and without ($Z=0$) an impurity,[16,17]—namely,

$$E_b(D^0) = E_0 - E(D^0). \tag{13}$$

Here, E_0 is the ground state of a single-electron QD without the impurity and $E(D^0)$ is the lowest level of the neutral donor. The binding energy of a D^- center is defined as

$$E_b(D^-) = E_0 + E(D^0) - E(D^-), \tag{14}$$

where $E(D^-)$ is the lowest level of the D^- center.[45,55]

The total energy is calculated by means of[40,53]

$$E = \sum_{i=1}^{N} \varepsilon_i - \frac{e}{2} \int \Phi_{e\text{-}e} \rho(r) d^3r + E_{xc}[\rho(r)] - \int V_{xc}[\rho(r)] \rho(r) d^3r. \tag{15}$$

The last two terms related to the XC potentials are taken as zero for only the Hartree approximation.

Figure 1 shows the variation of the binding energy of the D^0 and D^- centers, for cases with and without an XC potential, as a function of the dot radius. As seen from the figure, the binding energy of the D^0 is greater than that of the D^- impurity, because there is a repulsive Coulomb potential between the electrons, and so the second electron in the QD screens the influence of the attractive Coulomb potential of the impurity. The binding energies of the D^0 and the D^- with XC rise first with increasing dot radius and they reach maximum values, and then they decrease and reach the bulk values with further increasing of the dot radius. These binding energies become approximately constant asymptotically at

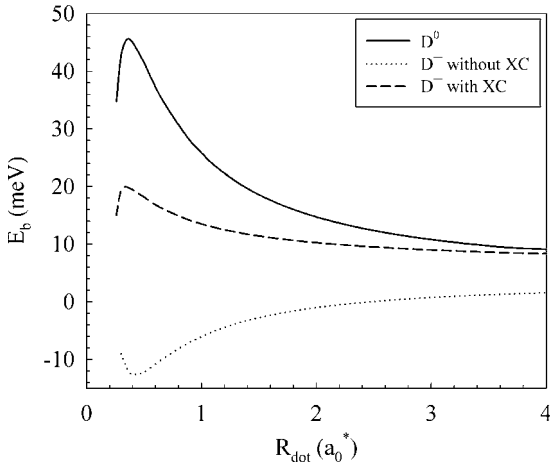

FIG. 1. Binding energy of the D^0 and D^- donor impurities as a function of the dot radius.

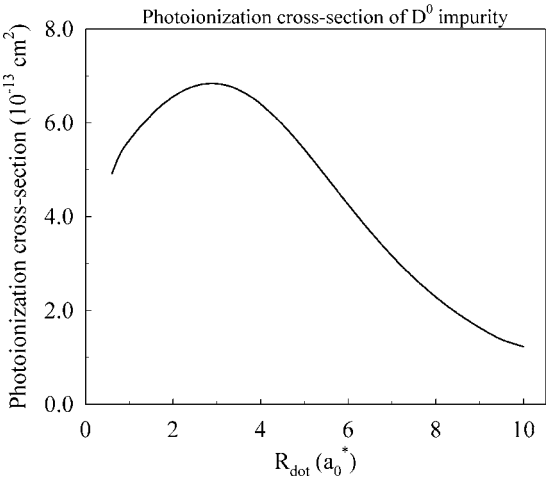

FIG. 2. Variation of the peak value of the photoionization cross section of the D^0 donor impurity with the radius.

larger radii. The results are in good agreement with the previous studies.[6,17,55–57] When the XC potential is not taken into account, the binding energy of the D^- becomes completely different as seen from Fig. 1. In this case, the binding energy of the D^- impurity has negative values up to $R_{dot}=2.5a_0^*$ and its general tendency looks antisymmetrical according to the D^- with XC potential case. This behavior is not in agreement with previously reported studies. The LDA works well and plays a significant role in two-electron systems. It is concluded that when the calculations of low-electron-density systems are carried out, the XC effects must be considered especially in electronic structure calculations.

A. Results of the photoionization cross section

In the peak values of the photoionization cross section, which take place when the photon energy is equal to the energy difference between initial and final energy states (i.e., threshold), all of the terms in Eq. (4), except the dipole matrix element and the photon energy $\hbar\omega$, contribute to photoionization merely a constant value. These terms do not have an effect on the shape of the photoionization cross section in the resonant case (i.e., $\hbar\omega=E_f-E_i$). In this case the $\delta(\hbar\omega-E_f-E_i)$ term becomes a constant, $1/\pi\hbar\Gamma$. However, the energy difference between the initial and final energy levels and also the overlapping of the wave functions of these levels determine the shape of the photoionization cross section. The overlapping is weak but the energy difference is large at very small QD radii. This is because the ground-state wave function of the impurity becomes localized near the dot center due to the attractive Coulomb potential of the impurity and, also, the excited energy level and its wave function in the QD without the impurity are generally in the continuum. But since the excited state becomes a bound state with increasing dot radius, the overlapping starts to rise. In further increasing of the QD radius, although there is not any limitation on the wave function of the excited state, the attractive Coulomb potential of the impurity brings some limitation on the ground-state wave function because of the same reason mentioned above. This process plays a negative role on the overlapping in large QDs. As a result, if the overlapping and energy difference are large, the photoionization cross section will be strong. In contrast, if the overlapping and energy difference is small, the photoionization will be small. Therefore, the behavior of the photoionization cross section gives some information about the overlapping of the wave functions.

In Fig. 2, the peak value of the photoionization cross section of the D^0 donor impurity is shown as a function of the dot radius for a finite potential barrier. The energy states and corresponding wave function for the D^0 impurity are determined by solving Eq. (1). It should be noted that the Coulomb potential between electrons and the many-body effects in Eq. (1) are taken as zero for the D^0 because of the single electron. As seen from the figure, first, the peak value increases with increasing radius, and then, it reaches a maximum value and decreases with a further increasing of the dot radius. This result is in good agreement with the previous studies.[21,50] According to the figure, initially, the photon energy is predominant in the photoionization cross section of the D^0 in small QD. As the difference decreases with increasing dot radius, the overlapping of the wave functions rises and reaches a maximum value of about $R_{dot}\cong 3.0a_0^*$. In this region, the overlapping is more dominant than the threshold photon energy. Although the energy difference and so the photon energy go to an approximately constant value (bulk value), the overlapping decreases with further increasing of the dot radius and it becomes weaker, and so photoionization gets small in large QDs.

Here, the photon polarization effect is not investigated because the photoionization cross section is independent of the photon polarization for an on-center impurity.[21]

The D^- impurity is more different from the D^0 because it contains two electrons. The Coulomb interaction between the electrons in the D^- must be taken into consideration. In addition, the XC effect can be also considered beyond the Hartree approximation. Figure 3 shows the peak value of the photoionization cross section of the one electron of the D^- donor impurity as a function of the QD radius. This calculation is performed for cases with and without exchange-

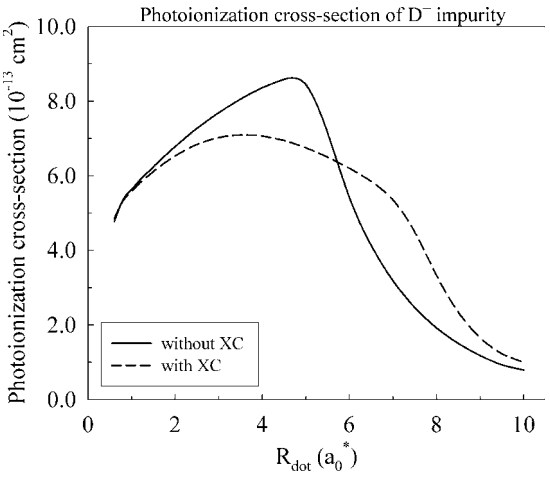

FIG. 3. The peak value of the photoionization cross section of the D^- donor impurity as a function of the radius with and without XC potential.

correlation term. As seen from the figure, the photoionization of the D^- center increases initially with increasing dot radius. Although the photoionization cross section reaches the maximum value at $R_{dot} \cong 3.0a_0^*$ when the XC potential is taken into account, it continues to increase up to $R_{dot} \cong 4.6a_0^*$ when the XC potential is neglected. In further increasing of the QD radius, while the photoionization with XC potential exhibits a smoother decreasing, it starts to fall down very fast in the case without the XC potential such that it lies under the photoionization with XC potential for $R_{dot} \geqslant 5.8a_0^*$.

As can be seen from the figure, the overlapping of the wave functions is quite strong up to $R_{dot}=4.6a_0^*$ when the XC potential is not considered in the calculation. After this point, the overlapping starts to be weak and it is to be very small with further increase in the dot radius. However, when the XC potential is taken into account, the overlapping becomes weaker. As seen from these results, the quantum-mechanical XC potential is to be more effective on the photoionization of the D^- center.

The photoionization of the D^- impurity is larger than that of the D^0. When the number of electrons grows in a QD, the absorption becomes stronger. Similar results were reported by Bondarenko and Zhao[12] in two-electron QDs for the absorption cross section.

Figure 4 shows the results of the photoionization cross section of the D^0 as a function of the normalized photon energy $\hbar\omega/(E_f-E_i)$ for different values of the dot radii. As seen from the figure, the maximum photoionization corresponds to the threshold photon energy and it decreases with increasing photon energy. The cross section rises first with increasing dot radii and then it decreases at much larger dot radii ($R_{dot} \geqslant$ about $4.0a_0^*$). This is clearly seen from inset and also Fig. 2. This behavior is not reported in previous studies because the photoionization cross section is not examined at very large dot radii. The reason for this behavior in large dot radii can be explained with the weak overlapping of the wave functions. When the radius of the QD goes to infinity, the photoionization threshold tends to its bulk value as expected.

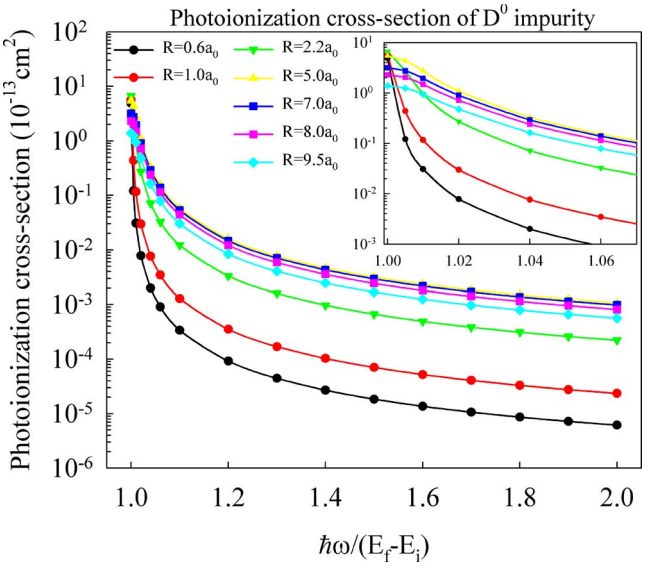

FIG. 4. (Color online) The photoionization cross section of D^0 as a function of the normalized photon energy for several dot radii.

Figure 5 shows the one-electron photoionization cross section of the D^- impurity as a function of the normalized photon energy for cases with and without exchange-correlation potential at different dot radii. Here, the maximum photoionization corresponds to the threshold photon energy and it decreases with increasing photon energy. The photoionization is to become larger in larger dot radii. However, at much larger dot radii ($R_{dot} \geqslant 5.0a_0^*$ without XC potential and $R_{dot} \geqslant 4.0a_0^*$ with XC potential) the photoionization cross section decreases. This behavior can be explained with weak overlapping and small energy difference in large QDs and also seen from Fig. 3.

The effect of the XC potential is seen clearly from Fig. 5. When the dot radius is small, the effectiveness of XC potential is to become less and the results for cases with and without XC are very close to each other. This effect is more prominent at large dot radii.

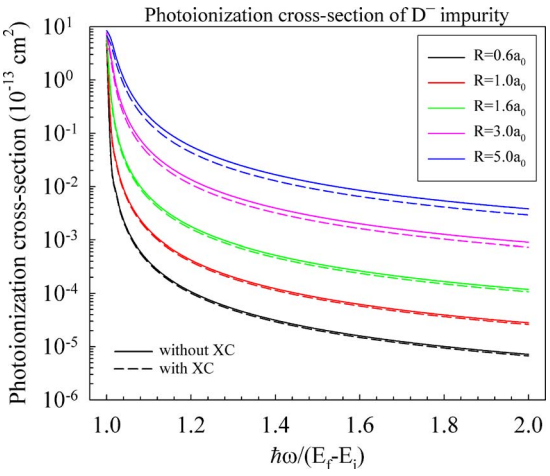

FIG. 5. (Color online) The photoionization cross section of D^- with and without XC potential as a function of the normalized photon energy for several dot radii.

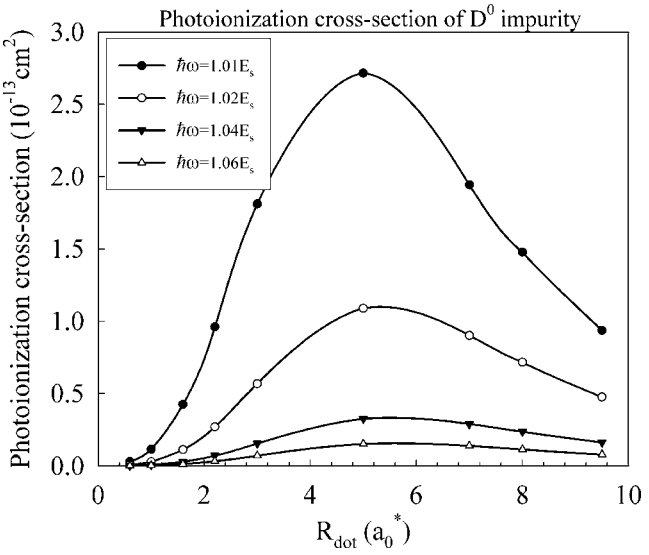

FIG. 6. The photoionization cross section of D^0 as a function of the dot radius for the normalized photon energy.

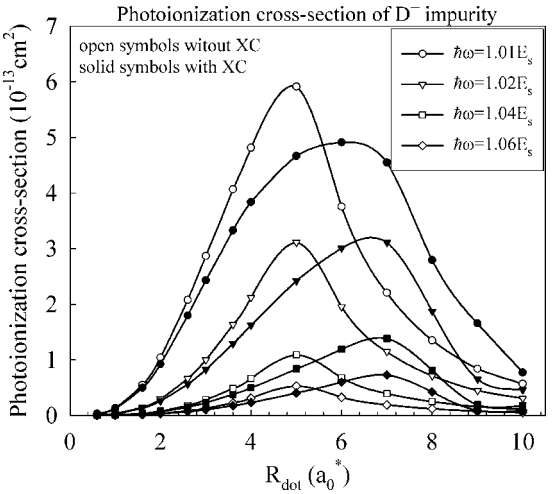

FIG. 7. The photoionization cross section of D^- with and without XC potential as a function of the dot radius for normalized photon energy.

As seen from Figs. 4 and 5, the maximum absorption occurs at the photoionization threshold and the photoionization cross section decreases monotonically from the maximum value with increasing photon energy like the true hydrogenic model for both D^0 and D^- cases. A similar result is reported for the photoionization of the D^0 impurity in a cubic QD.[30] This transition requires higher photon energies than in quantum wells and quantum wires. The reason for this behavior is that the electron is completely confined in all spatial dimensions in QD structures. This interesting result, which seems to be the characteristic and the signature of the QDs, is not exhibited in quantum well and quantum wire structures.[26,27,30,32,33,58,59] In these structures, although the threshold energy is in the confinement direction, some contribution comes from other free direction(s). As a result, the maximum absorption takes place at higher energies than the threshold energy in 2D and 1D structures.[26,27,32,33,58,59]

In Fig. 6, the variation of the photoionization cross section of the D^0 is plotted as a function of the dot radius for different normalized photon energies ($E_s=E_f-E_i$). As seen from the figure, first, the cross section goes up with increasing dot radius and then decreases again, after a maximum value, with further increasing of the dot radius. Also, while the photoionization is larger near the threshold energy, it becomes small at greater photon energies. Although the maximum value of the photoionization cross section is about $R_{dot}=4.0a_0^*$ for the threshold photon energy as seen from Fig. 2, it becomes about $R_{dot}=5.0a_0^*$ for greater photon energies (Fig. 6).

In Fig. 7, the variation of the photoionization cross section of the D^- is plotted as a function of the dot radius for different normalized photon energies ($E_s=E_f-E_i$) in cases with and without XC potential. The peak value of the photoionization grows initially with increasing dot radius, and it reaches a maximum value and then decreases again with further increasing of dot radius for both cases. The XC effect can be also seen clearly in this figure. While the photoionization cross-section value is larger at about $R_{dot}=5.0a_0^*$ for the case without an XC potential, it becomes larger at large dot radii ($6.0a_0^*<R_{dot}<7.0a_0^*$) for the case with an XC potential. In addition, as the photoionization cross section with XC potential is smaller at $\hbar\omega=1.01E_s$, it becomes the same as that without the XC potential case at $\hbar\omega=1.02E_s$, and then it becomes greater than that without the XC case at $\hbar\omega=1.04E_s$.

In off-resonant cases, not only dipole matrix element and photon energy but also $\delta(\hbar\omega-E_f-E_i)$ terms become effective on the shape of the photoionization cross section. Though the cross section is not explained as just overlapping of the wave functions and the photon energy, it can give some information about the overlapping.

In this context, as seen from Fig. 6, the overlapping of the wave functions is very strong near the threshold energy in the D^0 center and the overlapping becomes weaker with increasing photon energy. Namely, in off-resonant cases of the D^0, the photon energy becomes more dominant than the overlapping. Similar behavior is observed in the D^- center as seen from Fig. 7. However, while the overlapping with an XC potential is weaker than that without an XC potential near the threshold energy ($\hbar\omega=1.01E_s$), the overlapping with an XC potential becomes equal to that without an XC potential for $\hbar\omega=1.02E_s$. And the overlapping with the XC potential becomes stronger with higher photon energies.

B. Results of intersublevel transitions

Figures 8(a) and 8(b) show the ground and first excited electronic energy states of one- and two-electron QD with and without the impurity for different dot radii. The XC potential effect is also seen from Fig. 8(b) for two-electron cases. As seen from the figure, the electronic energy levels decrease with increasing dot radius for all cases. The dashed line shows the confining potential level. The bound levels for the $1p$ state start at $R_{dot}=0.5a_0^*$ in the $Z=0$ case for a single-electron QD, as those levels start at $R_{dot}=0.4a_0^*$ for the D^0.

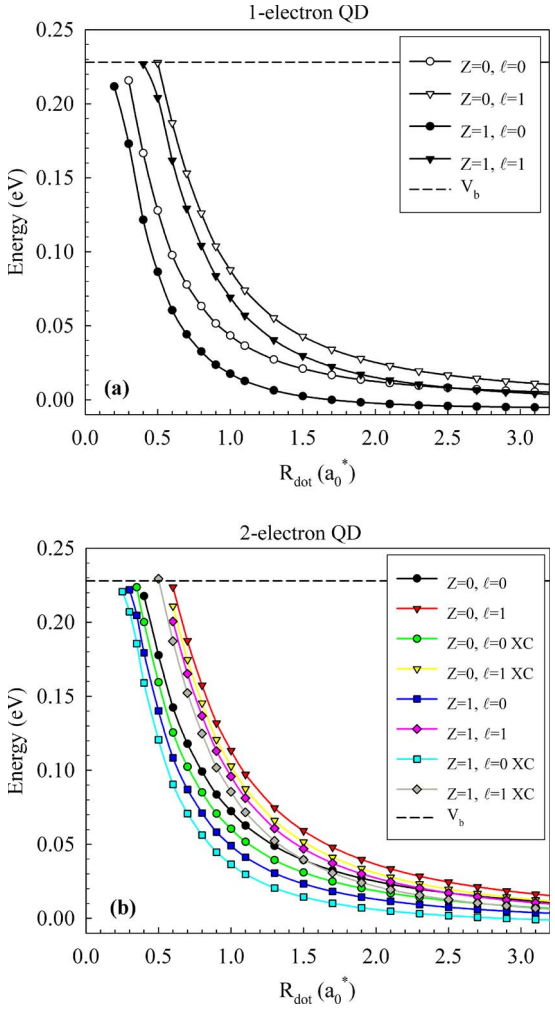

FIG. 8. (Color online) Energy levels of ground and first excited states as a function of dot radii (a) for a one-electron QD and (b) for a two-electron QD.

The $1p$ levels can be adopted as a quasibound level at these dot radii because these energy levels are approximately equal to the confining potential. The $1p$ energy state of the D^0 donor impurity lies under the $1s$ energy state of the case without an impurity for $R_{dot} > 2.5a_0^*$ because of the attractive Coulomb potential of the hydrogenic impurity. The $1s$ state of D^0 has negative energy eigenvalues for $R_{dot} > 1.5a_0^*$ and the attractive Coulomb potential begins to be more dominant than the kinetic energy. In this case, even if the confining potential is removed, the electron retains its own state and moves as bound to the attractive Coulomb potential of the impurity.

In the two-electron case, as seen from the Fig. 8(b), bound levels of the $1p$ state start at $R_{dot}=0.6a_0^*$ for both $Z=0$ and $Z=1$ cases. Only the $1p$ energy level of the D^- center stays on under the confining potential for $R_{dot} > 0.5a_0^*$ due to the XC potential effect adding to the attractive Coulomb potential of the impurity. The XC potential effect is seen clearly for both ground and excited states of $Z=0$ and $Z=1$ cases. The $1p$ energy level of the D^- with XC potential lies under the $1s$ level of $Z=0$ without and with XC one at $R_{dot} \geqslant 1.5a_0^*$ and $R_{dot} \geqslant 2.9a_0^*$, respectively.

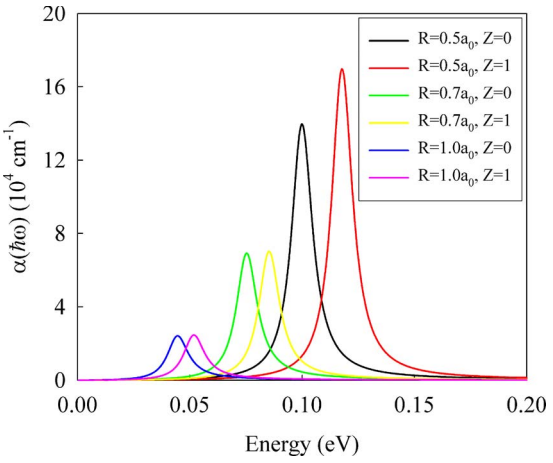

FIG. 9. (Color online) Absorption spectra of a one-electron QD as a function of the photon energy with and without impurity for three different dot radii.

In Fig. 9, the absorption spectra of a single-electron QD is seen as a function of photon energy for $Z=0$ and $Z=1$ cases and also for three different dot radii. The absorption spectra of small-radius QDs is much stronger than that of large-radius QDs because the absorption spectrum depends on the QD volume as $1/V_{QD}$, and so it changes with radius as $1/R^3$. Also, the absorption spectrum of D^0 is stronger than in the $Z=0$ case at smaller dot radii ($R_{dot}=0.5a_0^*$). The effect of the impurity seems clear. This effect vanishes with increasing dot radius and the absorption spectrum becomes the same as cases with and without an impurity. The absorption spectrum shifts to higher energies (blueshift) with impurity in all of the dot radii, because the attractive Coulomb potential pulls down the energy levels (especially $1s$), and so the energy difference between $1s$ and $1p$ levels becomes larger than in the $Z=0$ case.

The absorption peak wavelengths are 12.437, 16.514, and 27.781 μm for the $Z=0$ case and 10.549, 14.577, and 23.843 μm for the $Z=1$ case at $R_{dot}=0.5a_0^*$, $0.7a_0^*$, and $1.0a_0^*$, respectively. As seen from these values, this structure can be used for the fabrication of QDIPs in the long-wavelength infrared (LWIR) region. The differences between the absorption peak energies of the $Z=0$ and $Z=1$ cases are 17.86, 10, and 7.3 meV for $R_{dot}=0.5a_0^*$, $0.7a_0^*$, and $1.0a_0^*$, respectively. This difference is decreasing with increasing dot radius since the effect of the confining potential is reducing and, therefore, the energy values go to bulk values at large QD radii. The absorption spectrum peak values are decreasing with increasing dot radius, because the energy levels come close to each other and similar results have been reported by Jiang *et al.*[37]

The absorption spectra of a two-electron QD are shown in Fig. 10 as a function of the photon energy for three various dot radii. Here, the XC potential effect is also taken into consideration for both $Z=0$ and $Z=1$ cases as seen in Figs. 10(a) and 10(b), respectively. The absorption spectra of small QDs are much stronger than those of large QDs similar to single-electron QDs because of the same reason mentioned above. As seen from Figs. 10(a) and 10(b), the absorption

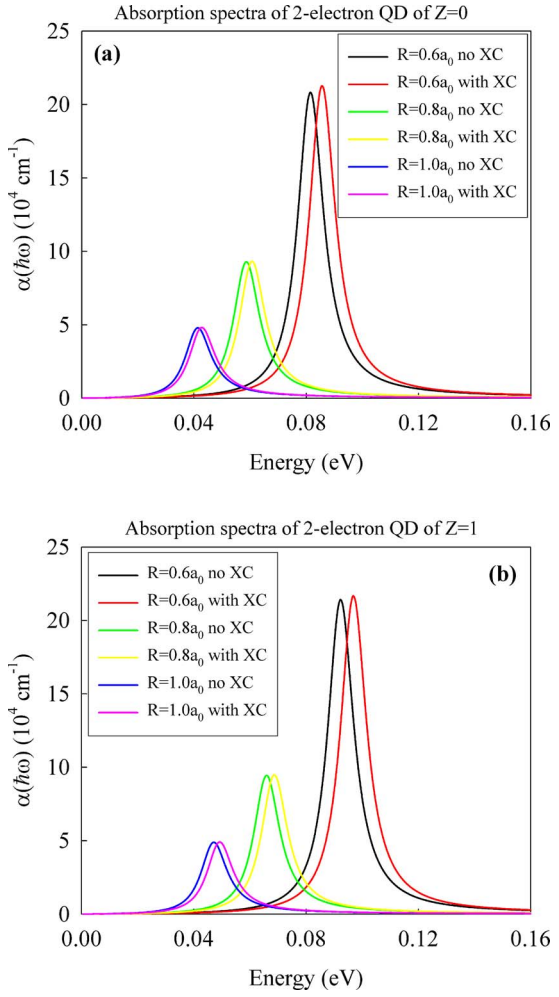

FIG. 10. (Color online) Absorption spectra of a two-electron QD as a function of the photon energy with and without XC potential for different radii (a) for $Z=0$ and (b) for $Z=1$ cases.

spectrum of a double-electron QD is more powerful than that of a single-electron QD as similar with previous studies.[12,60] The absorption spectrum shifts to higher energies (blueshift) with decreasing dot radii since the difference between energy levels increases with decreasing radius in both the $Z=0$ and $Z=1$ cases. The absorption peak wavelengths are 14.524 μm (15.264 μm), 20.538 μm (21.259 μm), and 28.967 μm (29.982 μm) for $Z=0$, and cases with (without) XC potential and 12.835 μm (13.470 μm), 18.128 μm (18.886 μm), and 25.111 μm (26.259 μm) for $Z=1$ and cases with (without) XC potential at $R_{dot}=0.6a_0^*$, $0.8a_0^*$, and $1.0a_0^*$, respectively. These values are also in the LWIR region.

The XC potential effect is more dominant at small dot radii. Some differences are observed in the absorption spectra with the XC potential for both cases. These differences are 4.14 meV (4.56 meV), 2.04 meV (2.74 meV), 1.45 meV (2.16 meV), and 0.63 meV (0.65 meV) for $Z=0$ ($Z=1$) and $R_{dot}=0.6a_0^*$, $0.8a_0^*$, $1.0a_0^*$, and $2.1a_0^*$, respectively. The difference is a bit more in the D^- center due to the attractive Coulomb potential of the impurity. The value of the absorption spectrum with XC potential is larger at small dot radii for both $Z=0$ and $Z=1$ cases. But this dependence on the XC potential is not very drastic. The absorption spectra shift to short wavelengths (blueshift) in the D^- according to the $Z=0$ case because, while the repulsive Coulomb interactions between electrons push the energy levels up especially the $1s$ state in the $Z=0$ case, the attractive Coulomb potential of the impurity pulls the energy states down in the $Z=1$ case and this effect is more dominant on the $1s$ state, and so the resonant energy between $1s$ and $1p$ states becomes a bit more than in the $Z=0$ case. Consequently, the absorption spectrum of the D^- center shifts to higher energies. Numerical values of this shifting are 11.25 meV (10.83 meV), 8.034 meV (7.335 meV), 6.58 meV (5.87 meV), and 2.57 meV (2.55 meV) at $R_{dot}=0.6a_0^*$, $0.8a_0^*$, $1.0a_0^*$, and $2.1a_0^*$, respectively, for case with (without) XC potential. As seen from the results, the differences decrease with increasing dot radius.

The surprisingly interesting result is that although the absorption peak energies correspond to energy differences between $1s$ and $1p$ states (threshold energy) at small dot radii, these peak energies become a bit larger than the threshold energies at large QD radii. This situation is observed in all cases. In single-electron dots, while the absorption peak energy is equal to the $1s$-$1p$ threshold energy at $R_{dot}=0.5a_0^*$ and $0.7a_0^*$, it becomes 44.680 meV (52.061 meV) for $Z=0$ ($Z=1$) at $R_{dot}=1.0a_0^*$ although the resonant energies are 44.239 meV (51.540 meV). In double-electron dots, as the absorption peak energy is equal to the resonant energy at $R_{dot}=0.6a_0^*$ and $0.8a_0^*$, it becomes 42.853 meV (41.402 meV) and 12.580 meV (11.951 meV) for $Z=0$ with (without) XC potential at $R_{dot}=1.0a_0^*$ and $2.1a_0^*$, respectively, in spite of the fact that the energy differences are 42.420 meV (40.991 meV) and 10.939 meV (10.388 meV). In the D^- center, the absorption peak energy values are 49.434 meV (47.271 meV) and 15.150 meV (14.502 meV) at $R_{dot}=1.0a_0^*$ and $2.1a_0^*$, respectively, for the case with (without) XC potential. However, the resonant energies in between the $1s$-$1p$ levels are 48.942 meV (46.798 meV) and 14.430 meV (13.180 meV) in the case with (without) XC potential for the same dot radii. As seen, this difference grows with increasing dot radius.

The oscillator strength is quite a useful parameter in order to get complementary information on electronic and optical properties of a QD. Two factors are effective on the oscillator strength. One of them is the energy difference between initial and final states, and the other one is overlapping of the wave functions of these two states as similar to the photoionization cross section. In small QDs, though the energy difference is very high, the overlapping is very small, and so the energy differences have a larger effect on the oscillator strength according to the dipole matrix elements. Increasing of the QD radius will increase the overlapping, as the energy differences are decreasing and, therefore, the dipole matrix element is more dominant on oscillator strength than the energy difference in large QDs.

Figure 11 shows the variation of the oscillator strength of the single-electron QD as a function of the dot radius for cases with and without an impurity. As seen from the figure, in the $Z=0$ case, the oscillator strength starts from 0.70 and rises very rapidly with increasing dot radius and it remains fixed about 0.97 after $R_{dot}>1.0a_0^*$ with further increasing of

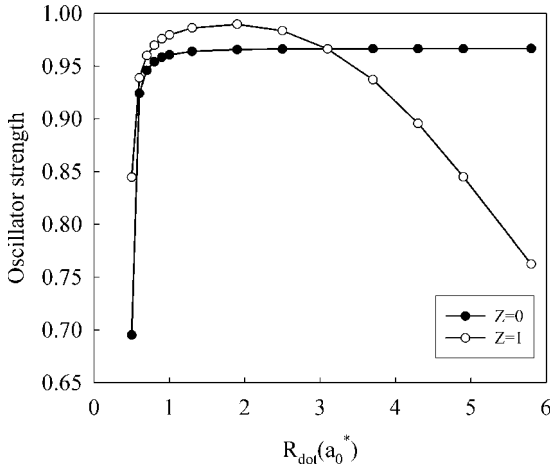

FIG. 11. Oscillator strength of the single-electron QD as a function of the QD radius with and without impurity.

the radius. While the energy differences decrease with increasing dot radius, the overlapping grows. As a result, the oscillator strength is to be fixed at a constant value in large QDs. In the $Z=1$ case, the oscillator strength begins from about 0.85 and it increases with increasing dot radius and reaches up to 0.98 values. It starts to decrease after $R_{dot} > 2.0a_0^*$ and continues to fall down rapidly with further increasing of the radius. These results are in good agreement with different studies.[11,13,37] A similar comment can be made for small and also large dot radii for this behavior. In large QD radii, the wave functions of the states, especially that of the $1s$ state, are localized near the center of the dot because of the attractive Coulomb potential of the impurity. And hence there is some limitation on the overlapping and the dipole matrix element has a constant value. Also the energy difference becomes less with increasing dot radius. As a result, the oscillator strength decreases in the $R_{dot} > 2.0a_0^*$ cases.

In Figs. 12(a) and 12(b), the variation of the oscillator strength of the double-electron QD is seen as a function of radius for $Z=0$ and $Z=1$ cases. The oscillator strength of a two-electron QD exhibits different behavior entirely from the single-electron case. The first difference is that the oscillator strength of the double-electron QD starts from much larger values in all cases than that of the single-electron QD. The oscillator strength of a two-electron QD for the $Z=0$ case increases very rapidly with increasing dot radius initially and then, after a peak value, it decreases again with further increasing of the dot radius. It has not got a fixed value as such in the one-electron case due to the Coulomb interaction between electrons. The repulsive Coulomb interaction between electrons brings not only a limitation on the overlapping but also closer energy levels to each other. Consequently, the oscillator strength decreases with further increasing of the QD radius in the $Z=0$ case. The oscillator strength of the D^- center, especially for case without a XC potential, is different from the double-electron QD without the impurity and also from the D^0. In the D^- without the XC potential, the oscillator strength is growing a little initially and continues increasing up to $R_{dot}=3.0a_0^*$ and then starts to smoothly decrease. It falls down very rapidly $R_{dot} > 5.0a_0^*$ with increasing dot radius. This behavior can be explained as follows: The attractive Coulomb potential of the impurity is screened somewhat by the repulsive Coulomb potential between the electrons. This process with contribution of the confining potential provides the overlapping at large QD up to a critical dot radius (here, $\approx 5.0a_0^*$), and in this range, the contribution of the dipole matrix element to the oscillator strength is much more than the transition energy. Hence, it becomes nearly fixed although the transition energy decreases. In further increasing of the radius, the effect of the confining potential becomes very weak and, therefore, both of the two electrons bind to the impurity and the overlapping of the wave functions starts to reduce. As a result, both transition energy and the overlapping decrease with further increasing of the dot radius. The XC potential effect can be also seen clearly from Fig. 12. In the $Z=0$ case, the oscillator strength with the XC potential is stronger than that without the XC potential case in all dot radii. As an exception to this behavior, the oscillator strengths with and without XC potential have the same trend. The XC potential effect is more different in the $Z=1$ case. As the oscillator strength with XC po-

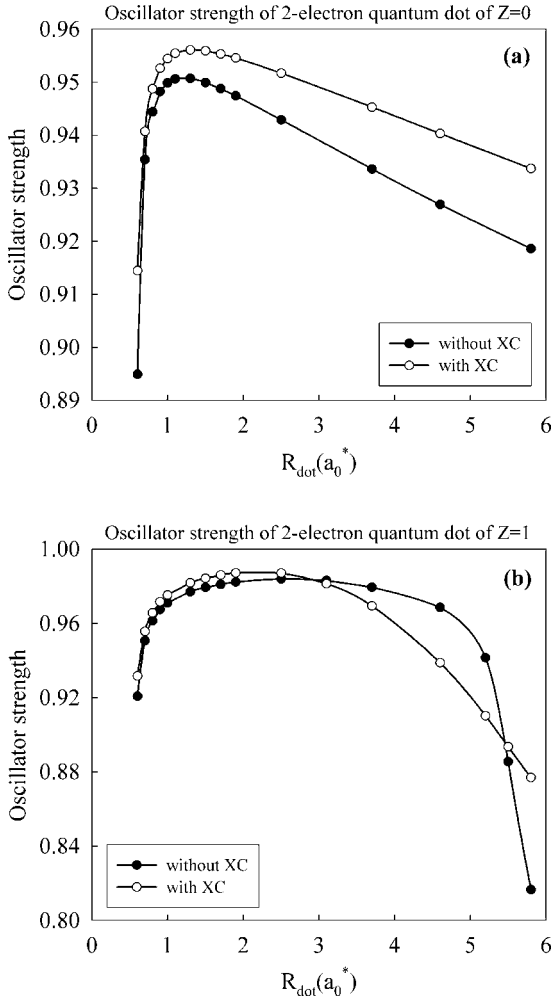

FIG. 12. Oscillator strength of the double-electron QD as a function of QD radius with and without XC potential (a) for $Z=0$ and (b) for $Z=1$ cases.

tential is a bit greater, it lies under the value of that without the XC one for $R_{dot} > 2.5a_0^*$ and then it is larger again than that without the XC potential one for $R_{dot} > 5.0a_0^*$. As a result, the XC potential has a serious effect on the overlapping of the wave functions.

IV. CONCLUSION

In this study, the detailed optical properties of one- and two-electron spherical QDs have been investigated using the matrix diagonalization technique for a finite confining potential well model. The many-body quantum mechanical XC effect has been also taken into account in the LDA for two-electron cases. The results obtained have been presented as a function of photon energies and dot radii.

The photoionization cross section has been computed for D^0 and D^- donor impurities in a spherical QD as a function of the dot radii and the normalized photon energies. The cross section is drastically dependent on the dot sizes and the photon energy for both D^0 and D^-. Also, the number of electrons in the QD affects the photoionization cross section. The effect of the XC term has also been investigated and it is seen that the photoionization cross section changes strongly with the XC potential. Therefore, many-body effects must be also taken into consideration in the calculation of the photoionization of many-electron systems.

Intersublevel transitions have been calculated in the same QD structures. It has been seen that the single-particle energy levels and the absorption spectra of the one- and two-electron QDs with and without the impurity are strongly affected by the QD radius in all cases. In the single-electron QD, the absorption spectrum of D^0 is stronger than that without an impurity. The absorption spectra are very robust in double-electron QDs with and without an impurity. The peak energies of the absorption spectrum of the QD with impurity shift to higher energies for both $N=1$ and $N=2$ cases. The interesting result is that the absorption peak energies are a bit greater than the threshold energies at large dots and this difference is to become more obvious with increasing dot radii. In addition, the XC potential effect on the absorption spectrum was carried out. The absorption peak energies with XC potential are separated from that without XC one for both the $Z=0$ and $Z=1$ cases. Moreover, the oscillator strength of single- and double-electron QDs have been investigated in both $Z=0$ and $Z=1$ cases and it seems that the oscillator strength is drastically affected by the number of electrons, existing in the impurity, many-body effects, and confining potential.

All results of the D^0 are in good agreement with previous theoretical studies.[11,21,30,34,50] To the best of our knowledge, for a D^- impurity, not only experimental reports related with the photoionization cross section or intersublevel transitions but also theoretical ones are not available for comparison of the results. I hope that this study will stimulate both experimental and theoretical investigations of the optical properties of the D^- centers. I think the results will also be very useful and contribute in understanding the optical properties of double-electron QDs with and without an impurity.

ACKNOWLEDGMENTS

This work was partially supported by Selçuk University BAP office. Also, I thank Marmaris Institute of Theoretical and Applied Physics (ITAP) for hospitality.

*sahinm@selcuk.edu.tr

[1] D. Bimberg, M. Grundmann, and N. N. Ledentsov, *Quantum Dot Heterostructures* (Wiley, Chichester, 1999).
[2] L. Jacak, P. Hawrylak, and A. Wojs, *Quantum Dots* (Springer-Verlag, Berlin, 1998).
[3] B. F. Levine, J. Appl. Phys. **74**, R1 (1993).
[4] V. Ryzhii, Semicond. Sci. Technol. **11**, 759 (1996).
[5] S.-W. Lee, K. Hirakawa, and Y. Shimada, Physica E (Amsterdam) **7**, 499 (2000).
[6] M. Şahin and M. Tomak, Phys. Rev. B **72**, 125323 (2005).
[7] M. Şahin and M. Tomak, Physica E (Amsterdam) **28**, 247 (2005).
[8] J. I. Lee, H. G. Lee, E.-J. Shin, S. Yu, D. Kim, and G. Ihm, Appl. Phys. Lett. **70**, 2885 (1997).
[9] S.-W. Lee, K. Hirakawa, and Y. Shimada, Appl. Phys. Lett. **75**, 1428 (1999).
[10] S.-S. Li and J.-B. Xia, Phys. Rev. B **55**, 15434 (1997).
[11] R. Buczko and F. Bassani, Phys. Rev. B **54**, 2667 (1996).
[12] V. Bondarenko and Y. Zhao, J. Phys.: Condens. Matter **15**, 1377 (2003).
[13] S. Yilmaz and H. Şafak, Physica E (Amsterdam) **36**, 40 (2007).
[14] V. Milanovic and Z. Ikonic, Phys. Rev. B **39**, 7982 (1989).
[15] R. L. Greene and K. K. Bajaj, Solid State Commun. **45**, 825 (1983).
[16] J.-L. Zhu, J.-J. Xiong, and B.-L. Gu, Phys. Rev. B **41**, 6001 (1990).
[17] N. Porras-Montenegro and S. T. Perez-Merchancano, Phys. Rev. B **46**, 9780 (1992).
[18] H. Şafak, M. Şahin, B. Gülveren, and M. Tomak, Int. J. Mod. Phys. C **14**, 775 (2003).
[19] A. J. Peter, Mod. Phys. Lett. B **20**, 1127 (2006).
[20] Z. X. Jiang, B. D. McCombe, and P. Hawrylak, Phys. Rev. Lett. **81**, 3499 (1998).
[21] H. Ham and H. N. Spector, J. Appl. Phys. **93**, 3900 (2003).
[22] M. Lax, in *Proceedings of the 1954 Atlantic City Conference on Photoconductivity*, edited by R. G. Breckenridge, B. R. Russell, and E. E. Hahn (Wiley, New York, 1956).
[23] M. Takikawa, K. Kelting, G. Brunthaler, M. Takeshi, and J. Komena, J. Appl. Phys. **65**, 3937 (1989).
[24] K. F. Ilaiwi and M. Tomak, J. Phys. Chem. Solids **51**, 361 (1990).
[25] M. El-Said and M. Tomak, J. Phys. Chem. Solids **52**, 603 (1990).
[26] M. El-Said and M. Tomak, Solid State Commun. **82**, 721 (1992).
[27] M. I. El-Kawni and M. Tomak, Surf. Sci. **260**, 319 (1992).
[28] K. F. Ilaiwi and M. El-Said, Phys. Status Solidi B **187**, 93 (1995).
[29] A. Sali, M. Fliyou, and H. Loumrhari, Physica B **233**, 196 (1997).
[30] A. Sali, H. Satori, M. Fliyou, and H. Loumrhari, Phys. Status Solidi B **232**, 209 (2002).
[31] H. Ham and C. J. Lee, J. Appl. Phys. **96**, 335 (2004).

[32] E. Kasapoglu, H. Sari, U. Yesilgul, and I. Sokmen, Surf. Rev. Lett. **11**, 411 (2004); J. Phys.: Condens. Matter **18**, 6263 (2006).
[33] E. Kasapoglu, U. Yesilgul, H. Sari, and I. Sokmen, Physica B **368**, 76 (2005).
[34] J. D. Correa, O. Cepeda-Giraldo, N. Porras-Montenegro, and C. A. Duque, Phys. Status Solidi B **241**, 3311 (2004).
[35] H. Ham and H. N. Spector, J. Appl. Phys. **100**, 024304 (2006).
[36] J. D. Correa, N. Porras-Montenegro, and C. A. Duque, Braz. J. Phys. **36**, 387 (2006).
[37] X. Jiang, S. S. Li, and M. Z. Tidrow, Physica E (Amsterdam) **5**, 27 (1999).
[38] J. L. Gondar and F. Comas, Physica B **322**, 413 (2002).
[39] N. Vukmirovic, Z. Gacevic, Z. Ikonic, D. Indjin, P. Harrison, and V. Milanovic, Semicond. Sci. Technol. **21**, 1098 (2006).
[40] R. G. Parr and W. Yang, *Density Functional Theory of Atoms and Molecules* (Oxford University Press, Oxford, 1989).
[41] E. A. Johson, in *Low Dimensional Semiconductor Structures*, edited by K. Barnham and D. Vvedensky (Cambridge University Press, Cambridge, England, 2001), p. 79.
[42] V. V. Mitin, V. A. Kochelap, and M. A. Stroscio, *Quantum Heterostructures* (Cambridge University Press, Cambridge, England, 2001).
[43] G. Bastard, *Wave Mechanics Applied to Semiconductor Heterostructures* (Les Editions de Physique, Paris, 1988).
[44] J. See, P. Dollfus, and S. Galdin, J. Appl. Phys. **92**, 3141 (2002).
[45] R. K. Pandey, M. K. Harbola, and V. A. Singh, Phys. Rev. B **70**, 193308 (2004).
[46] Ş. Erkoç, in *Annual Reviews of Computational Physics IX*, edited by D. Stauffer (World Scientific, Singapore, 2001), p. 5.
[47] J. P. Perdew and A. Zunger, Phys. Rev. B **23**, 5048 (1981).
[48] D. M. Ceperley and B. J. Alder, Phys. Rev. Lett. **45**, 566 (1980).
[49] B. K. Ridley, *Quantum Process in Semiconductors* (Clarendon Press, Oxford, 1982).
[50] H. Ham and C. J. Lee, J. Korean Phys. Soc. **42**, S688 (2003).
[51] J. S. de Sousa, J.-P. Leburton, V. N. Freire, and E. F. da Silva, Phys. Rev. B **72**, 155438 (2005).
[52] S. Adachi, J. Appl. Phys. **58**, R1 (1985).
[53] J. M. Thijssen, *Computational Physics* (Cambridge University Press, Cambridge, England, 1999).
[54] D. Chandramohan, S. Balasubramanian, and M. Tomak, Phys. Rev. B **37**, 7102 (1988).
[55] J.-L. Zhu, J.-H. Zhao, W.-H. Duan, and B.-L. Gu, Phys. Rev. B **46**, 7546 (1992).
[56] Z.-Y. Deng, J.-K. Gou, and T.-R. Lai, J. Phys.: Condens. Matter **6**, 5949 (1994).
[57] J.-L. Zhu, J.-H. Zhao, and J.-J. Xiong, Phys. Rev. B **50**, 1832 (1994).
[58] A. Sali, M. Fliyou, L. Roubi, and H. Loumrhari, J. Phys.: Condens. Matter **11**, 2427 (1999).
[59] A. Sali, M. Fliyou, H. Satori, and H. Loumrhari, J. Phys. Chem. Solids **64**, 31 (2003).
[60] A. Weber, O. Gauthier-Lafaye, F. H. Julien, J. Brault, M. Gendry, Y. Desieres, and T. Benyattou, Appl. Phys. Lett. **74**, 413 (1999).